Nanoparticle-Assisted Multilayered Photothermal Therapy Concerning Countercurrent Blood Flow: A Numerical Study

Abhijit Paul and Anup Paul

Nomenclature

t	Laser exposure time (s)
R	Beam radius (mm)
D	Diameter of rod (m)
s	Number of nanoparticles per unit volume, (m^{-3})
T	Temperature (°C)
Q	Vomumetric heat generation rate (W/m^3)
U	Universal gas constant (J/mol K)
C_d	Damaged concentration of protein
C_0	Undamaged concentration of protein
∇	Gradient
v	Blood flow velocity
C	Specific heat (J/kg K)
k	Thermal conductivity (W/m K)
x, y, z	Coordinates (mm)
I_0	Irradiated laser intensity (W/m^2)
ω_b	Blood perfusion rate (s^{-1})
Ω	Damage integral
h	Ambient convective heat transfer coefficient, (W/m^2 K)
G	Activation energy (J/mol K)
A	Pre-exponential factor (s^{-1})
P	Pressure (Pa)
S	Thermophysical and optical properties
p, n	Consistency and power law index
q	Heat flux
f	Volume force

A. Paul · A. Paul (✉)
Department of Mechanical Engineering, NIT Arunachal Pradesh, Yupia 791112, India

P. Mahanta et al. (eds.), *Advances in Thermofluids and Renewable Energy*, Lecture Notes in Mechanical Engineering, https://doi.org/10.1007/978-981-16-3497-0_7

Greek Symbols

η	Volumetric concentration (dimensionless)
ρ	Density (kg/m^3)
ψ	Shear stress in blood medium
τ_q	Heat flux phase lag
τ_T	Temperature gradient phase lag
α	Absorption coefficient (m^{-1})
β	Scattering coefficient (m^{-1})

Subscripts

amb	Ambient
np	Nanoparticle
mix	Mixture
met	Metabolic
perf	Perfusion
b	Blood
t	Tissue

Abbreviations

IT	Intratumoral
IV	Intravenous
IR	Infrared
AuNs	Gold nanoshells

1 Introduction

Day by day cancer has turned out to be a worldwide threat for humankind. Nowadays, skin cancer exhibits a common cause of cancer deaths. Thus, the study of various cancer treatment methods is the prime focus of most researchers. Light sensitive agent-assisted photothermal therapy has arrived as an effective treatment procedure, applying laser technology.

The laser is a collimated, coherent and monochromatic source of light. Therefore, laser is one of the best tools [1–4] for treating cancer precisely either directly or via optical catheter. During photothermal therapy in clinic, surgeons often face difficulties in proper assessment of the extent of thermal ablation. Thus, the computational

justification of a certain prototype before real clinical application often enhances the clinical safety.

In spite of many advantages, the complete acceptance of laser technology in noninvasive cancer treatments is still a challenge [1] due to the limitations of unfocused energy diffusion. Various works have been executed on precise thermal damage of tumor, preserving the surrounding healthy tissues. Recently laser-based photothermal therapy incorporating nanotechnology has drawn a wider focus. During the infusion of nanoparticles through veins, most of the particles get entrapped [2] in other organs despite the targeted zone. Hence, it is a challenge to deliver the nanoparticles properly to the targeted site during intravenous infusion scheme. Literature [1, 2] shows that the intratumoral infusion scheme of nanoparticles dominates over intravenous infusion scheme during laser therapy.

Different heat transmission models are applied by various authors [5, 6] to predict thermal behavior of bio-tissues under external agitation. Pennes bioheat model is the most popular model considering heat transmission at an infinite speed, although this model is a deficit of accurate prediction within inhomogenous tissue medium. The biological tissue medium exhibits a non-Fourier thermal behavior with heat propagation at a finite speed. Many authors have witnessed a fluctuating thermal history [7, 8] in nonhomogeneous tissue medium applying non-Fourier DPL model. In fact, several researchers have revealed accurate thermal prediction in the case of DPL model compared to classical heat transfer model. For accurate prediction of thermal history in biological tissue, it is also very important to incorporate blood vessels in the heat transfer model. Additionally, the metabolic effect in human body exhibits a heat source during photothermal treatment. In Pennes bioheat model, the effect of all micro capillaries has been considered as a scalar blood perfusion term.

The present literature explains about the nanoparticle-based photothermal behavior of tissues during laser-assisted noninvasive cancer treatment. However, studies so far have failed to predict the thermal effect of biological tissues under the intratumoral infusion scheme of nanoparticles considering the countercurrent blood flow within multilayer tissue model. Therefore, in present work, an attempt has been executed to analyze the thermal response in triple-layered tissue model infusing gold nanosphere embedded in countercurrent blood vessel. The prime aim is to perform a comparative study between intratumoral and intravenous infusion schemes of nanoparticles in terms of localized thermal heating of targeted region, sparing the surrounding healthy tissue. Both Pennes and dual-phase lag bioheat model are applied to analyze the heat transfer process within the respective tissue model. Besides, the non-Newtonian power law has been utilized for analyzing the heat transfer of blood flow.

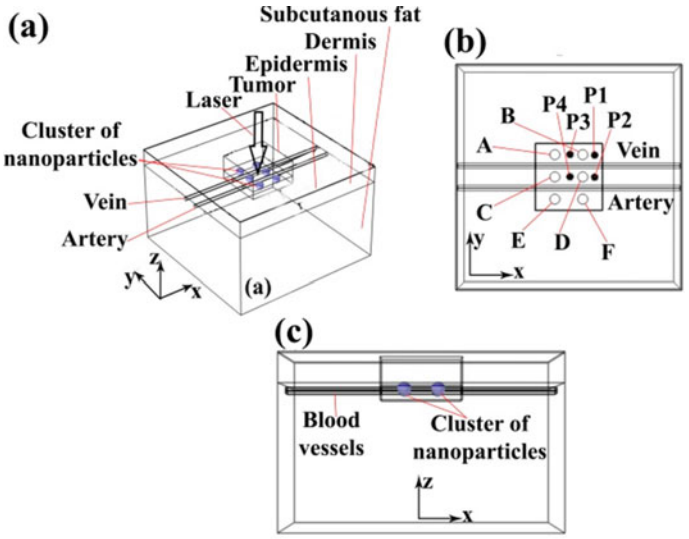

Fig. 1 Demonstration of the computational domain **a** Isometric view **b** top view, **c** side view, where A, B, C, D, E and F denote the cluster of nanoparticles

2 Mathematical Model

2.1 Physical Domain

A three-dimensional triple-layered tissue model has been selected for the present numerical study and is shown in Fig. 1. The dimensions and various optical and thermal properties of tissue model are given in Table 1 which are collected from various references [10–13]. The blood vessels bear a radius of 0.24 mm and are located at a depth of 2.4 mm from tissue top surface. The radius of each AuNp clusters are chosen to be 0.5 mm [10–12] and respective locations are given as A, B, C, D, E and F in the model and is expressed as (x, y, z): (−1.25, 2, −2.3); (1.25, 2, −2.3); (−1.25, 0, -2.3); (1.25, 0, −2.3); (−1.25, −2, −2.3); (1.25, −2, −2.3), respectively, in mm. P1, P2, P3 and P4 are indicated in Fig. 1b as (x, y, z): (2, 2, 0), (2, 0, 0), (0, 2, 0), (0, 0, 0) for the following discussion.

2.2 Physical Description

To analyze the thermal response of tissue under laser heating, a transient heat transfer momentum equation is solved simultaneously considering various initial and boundary conditions. To simplify the problem, the following assumptions are considered.

Table 1 Dimensions and physical properties of tissue medium [10–12]

	Subcutaneous fat	Dermis	Epidermis	Tumor	AuNs
Width and breadth (mm)	20	20	20	6	–
Thickness (mm)	10	2	0.08	3	–
Density, ρ (kg/m^3)	1210	1090	1200	1030	19,320
Thermal conductivity, k (W/m K)	0.194	0.42	0.24	0.558	317
Specific heat, C (J/kg K)	2240	3350	3950	3582	128
Blood perfusion, ω_b (1/s)	0.0031	0.0031	0	0.0063	–
Metabolic heat generation rate, Q_{met} (W/m^3)	368	368	368	3680	–
Scattering coefficient, b (1/m), 549 nm	5	5	5	500	45.94×10^6
Absorption coefficient, a (1/m), 549 nm	0.24	0.24	0.9	80	67.88×10^6

1. Constant thermal and optical properties of the tissue medium.
2. No phase change and chemical reaction within the tissue domain.
3. Smooth condition at the interface of each tissue layer.
4. Isotropic tissue medium.
5. Laminar and incompressible blood flow.

The classical bioheat equation of Pennes is given as,

$$\rho C \frac{\partial T}{\partial t} = -\nabla \cdot q(r, z, t) + \rho_b C_b \omega_b (T_b - T) + Q_{\text{met}} + Q_{\text{laser}}(r, z) \tag{1}$$

$$q(r, z, t) = -k \nabla T(r, z, t) \tag{2}$$

where ρ is the tissue density (kg/m^3), C is the tissue capacity of heat at constant pressure (J/kg K), k is the thermal conductivity (W/m K) of tissue, T is the temperature (°C) of tissue domain, ω_b is the blood perfusion rate (1/s), the subscript b defines blood domain, Q_{met} is the heat generation rate of metabolism, Q_{laser} is the term of external heat source (W/m^3).

The deposition of external heat ($Q_{\text{laser}}(r, z)$) is formulated by the modified Beer–Lambert law, given as,

$$Q_{\text{laser}}(r, z) = \alpha I_0 \exp\left\{ \frac{-r^2}{2(R(0))^2 \exp(\beta z)} \right\} \exp\{-(\alpha + \beta) z\} \tag{3}$$

$$r = \sqrt{x^2 + y^2} \tag{4}$$

where I_0 is the laser energy intensity at upper surface of the tissue in W/m^2, $R(0)$ is the beam radius at tissue upper surface ($r, z = 0$), α, β are the coefficient of absorption

and scattering, respectively. In present study, I_0 is taken as 32,000 W/m^2 whereas $R(0)$ is taken as 2.5 mm [10].

The DPL model in Cartesian coordinate form can be expressed as,

$$q(x, y, z, t + \tau_q) = -k\nabla T(x, y, z, t + \tau_T) \tag{5}$$

Applying divergence of Eq. (5) and placing $\nabla \cdot q$ in Eq. (1), the DPL model can be expressed as

$$\begin{aligned} \tau_q \rho C \frac{\partial^2 T}{\partial t^2} + \left(\tau_q \omega_b \rho_b C_b + \rho C\right) \frac{\partial T}{\partial t} = k\nabla^2 T + \tau_T k \nabla^2 \frac{\partial T}{\partial t} + \\ \omega_b \rho_b C_b (T_b - T) + Q_{\text{laser}} + Q_{\text{met}} + \tau_q \frac{\partial Q_{\text{met}}}{\partial t} + \tau_q \frac{\partial Q_{\text{laser}}}{\partial t} \end{aligned} \tag{6}$$

where τ_q and τ_T define the phase lags due to heat flux and temperature gradient, respectively. For both healthy tissue and tumor section, τ_q and τ_T are considered as 16 s and 0.043 s, respectively, and the same for AuNs is considered as 0.744 ps and 89.28 ps, respectively [10]. A constant value of τ_q and τ_T is considered for all the layers of tissue.

The changed thermophysical and optical properties of tissue due to the doping of gold nanospheres (AuNp) ($r = 40$ nm) are addressed applying Eqs. (7) and (8) for the case of IV only [14].

$$S_{\text{mix}} = \eta S_{\text{np}} + (1 - \eta) S_t \tag{7}$$

$$\frac{1}{k_{\text{mix}}} = \frac{\eta}{k_{\text{np}}} + \frac{1 - \eta}{k_t} \tag{8}$$

where η is the volume concentration of nanoparticles and can be expressed by the below relation mentioning the total number of AuNp per unit volume (s) and radius of AuNp (r_{np}), respectively.

$$\eta = s\left(\frac{4\pi r_{\text{np}}^3}{3}\right) \tag{9}$$

In the present work, η for the intravenous case is considered as 3.6×10^{-5} [11]. On the other hand, for the IT scheme, the AuNp clusters are taken as subdomains into the tissue domain and the bioheat equation is computed individually.

The initial condition of temperature within the tissue domain is

$$T_i(x, y, z, 0) = 37\ ^\circ\text{C} \tag{10}$$

The upper plane of the tissue ($z = 0$) is given to be Fourier convective boundary condition for the Fourier model (Eq. 1) and the non-Fourier convective boundary

condition for the DPL model (Eq. 16), respectively

$$-n.(-k\nabla T) = h_{\text{amb}}(T_{\text{amb}} - T) \tag{11}$$

$$-n.\left(-k\nabla T - \tau_T k\nabla\frac{\partial T}{\partial t}\right) = h_{\text{amb}}\left(T_{\text{amb}} - T - \tau_q\frac{\partial T}{\partial t}\right) \tag{12}$$

The remaining planes are kept to be adiabatic

$$-n.(-k\nabla T) = 0 \tag{13}$$

The velocity and temperature of blood flow have been computed from the following equations,

$$\nabla \cdot v = 0 \tag{14}$$

$$\rho\left(\frac{\partial v}{\partial t} + v \cdot \nabla v\right) = -\nabla p + \nabla \cdot \Gamma + f \tag{15}$$

$$\rho C_b\frac{\partial T}{\partial t} + \rho C_b v \cdot \nabla T = \nabla \cdot (k\nabla T) + Q_{\text{laser}}(r, z) \tag{16}$$

where v, ρ, Γ, p, f are velocity, density, stress tensor, pressure and body force term, respectively, whereas $Q_{\text{laser}}(r, z)$ is the applied external heat source (Eq. 3).

The non-Newtonian power law for the blood flow is expressed by the following [11] shear stress (ψ), given as

$$\psi_{xy} = p\left(\frac{\mathrm{d}v}{\mathrm{d}y}\right)^n = p\left|\frac{\mathrm{d}v}{\mathrm{d}y}\right|^{n-1}\frac{\mathrm{d}v}{\mathrm{d}y} \tag{17}$$

where n and p are power law index and consistency, respectively.

In the present problem, the blood velocity at the inlet of artery and vein is kept as 0.03 m/s [11]. Whereas the temperature at the inlet section of artery and vein is given as 37 °C. The outlet pressure of the blood vessels is kept as 80 mm of Hg.

The damage parameter (Ω) [15] has been expressed as,

$$\Omega = \ln\left(\frac{C_0}{C_0 - C_d}\right) \tag{18}$$

where C_0 is the concentration of protein in healthy tissue,C_d is the damaged concentration of protein after therapy. The denaturation of protein happens at $\Omega \geq 0.53$[11], whereas the permanent cell death happens at $\Omega \geq 1$. The results of the DPL bioheat model are applied to compute the damage integral applying the Arrhenius equation. The thermal damage rate can be defined as

$$\frac{d\Omega}{dt} = Ae^{(-G/UT(x,y,z,t))} \tag{19}$$

where G is the energy of activation, considered as 6.28×10^5 J/mol, U is the universal gas constant in J/mol K, T is the tissue temperature in K, A is the pre-exponential factor which is taken as 3.1×10^{98} s^{-1}.

2.3 Numerical Scheme and Validation

In the present study, the bioheat equations were computed by applying finite element method using COMSOLTM Multiphysics software. The present computational results were validated with the previous Paul et al. [11] experimental results and are shown in Fig. 2.

3 Results and Discussion

To analyze the thermal characteristics of tissue infusing nanoparticles (AuNp) under laser therapy, two separate schemes, viz. intravenous (IV) and intratumoral (IT), have been implemented in the present work. The simulated domain becomes more realistic with triple-layered tissue structure embedding countercurrent blood flow. The consequence of two different nanoparticle infusion techniques in terms of localized thermal damage of tumor preserving the surrounding healthy tissue, considering the role of blood flow through artery and vein under external laser irradiation has been analyzed numerically. The thermal phase lag of biological tissue to respond to external heating has been simulated in the current bioheat model by applying dual-phase lag (DPL) model.

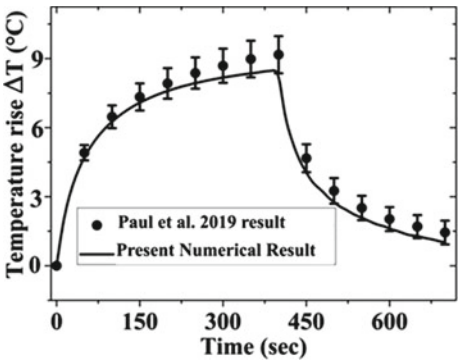

Fig. 2 Variation of predicted (present study) and measured [6] temperature difference with respect to time in the tissue medium

3.1 *Thermal Response of Tissue Under Localized Nanoparticle Injection*

The spatial temperature history within the malignant and normal tissue has been computed to predict the span of identical necrosis into the tumor site under external heating. The 2-D temperature plot on x–y plane at various positions (e.g., $z = 0$, -1 mm, -2 mm, -3 mm) with respect to tissue upper plane for the schemes of IV and IT at $t = 300$ s is depicted in Fig. 3. The utmost temperature of x–y plane at $z = 0$, -1 mm, -3 mm and -4 mm are revealed to be 71.4 °C, 50 °C, 44 °C and 42°C for IV and 56 °C, 58 °C, 71.4 °C and 63 °C for IT, respectively. The plasmonic effect at the surface of the gold nanoparticles under external laser heating implies a fast conversion of exterior light energy to heat energy subsequently dissipating the same to the neighboring normal tissue. The extent of threshold temperature profile ($T >$

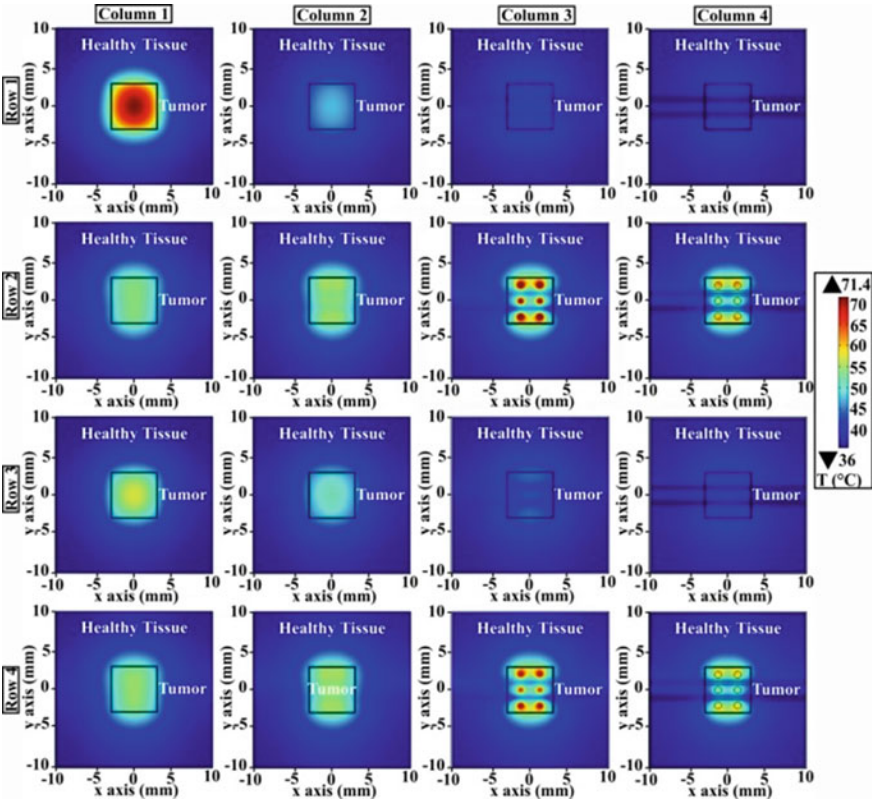

Fig. 3 Tissue temperature history on x–y plane at different depths of $z = 0$ mm [Column 1], $z = -1$ mm [Column 2], $z = -2$ mm [Column 3], $z = -3$ mm [Column 4], for different schemes of IV [Row 1 and 3] and IT [Row 2, 4] applying Pennes [Row 1 and 2] and DPL [Row 2 and 4] model at $t = 300$ s

50 °C) [15] has been revealed to be gradually diminished with the increasing depth for the scheme of IV (Fig. 3 [Row 1 and 3]) ensuing a nonuniform profile of necrosis along the depth of tumor. In case of IV, the absorption of applied laser energy within the tissue domain progressively decreases its power along its path. A uniform profile of necrotic temperature has been revealed in the whole tumor in case of IT (Fig. 3 [Row 2 and 4]). The tumor confined gathering of nanoparticles provides an option in the case of IT to accumulate the photon energy up the tumor's lower surface unlike decreasing its power due to diffusion. Moreover, the countercurrent blood flow with the interior body temperature of 37 °C affects a significant heat loss within the tissue structure for the cases of IV in comparison to IT as shown in Fig. 3. During the intratumoral doping scheme, the gathered AuNp attains more photon energy into itself causing a targeted temperature raise at the cluster regime thereby diminishing the heat sink effect of blood vessels.

The resulting extent of necrosis obtained within the tissue model for the schemes of IV and IT has been explored by showing the necrotic damage integral contour ($\Omega \geq 1$) [16]. The corresponding 2-D necrotic damage profile on x–y plane at various depths are depicted in Fig. 4 for $t = 300$ s. A uniform damage of tumor preserving the neighboring normal tissue has been revealed during the IT infusion scheme of AuNp in contrast to the scheme of IV. For intravenous doping, it is considered that the nanoparticles are homogenously spread into the entire tumor section which results the dissipation of heat energy to the surrounding normal tissues. On the other hand, during intratumoral doping, the existence of nanoparticles in accumulated form results in binding the heat energy and thereby dissipating the same to the neighboring

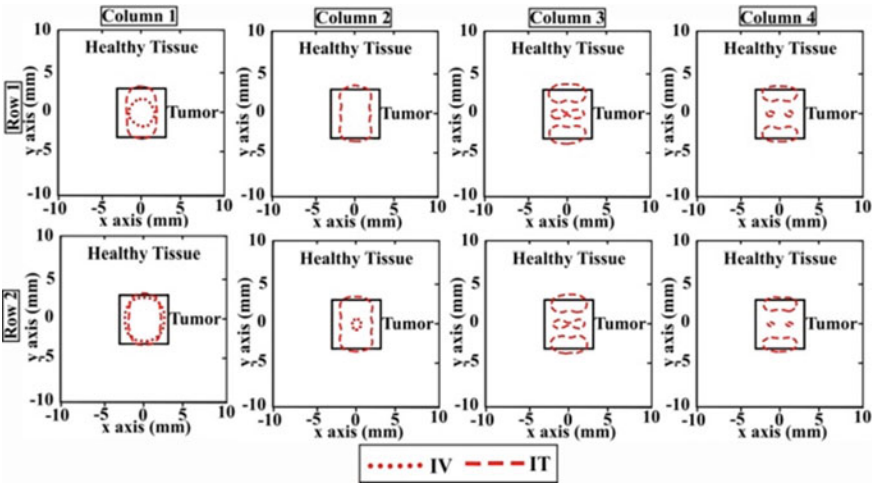

Fig. 4 Necrotic damage contour plots of tissue on x–y plane at different depths of $z = 0$ mm [Column 1], $z = -1$ mm [Column 2], $z = -2$ mm [Column 3], $z = -3$ mm [Column 4] applying Pennes [Row 1] and DPL [Row 2] model under different infusion schemes of nanoparticles, viz. IV and IT at $t = 300$ s

tumor regime. Thus, the targeted injection technique of AuNp in the scheme of IT affects a more uniform and concise ablation of tumor in contrast to the IV scheme.

3.2 *Effect of Non-fourier Bioheat Model Over the Fourier Model*

To explore the inhomogeneous nature of tissue model in the presence of large blood vessel incorporating clusters of nanoparticles under laser illumination, the variation of the temperature history with the exposure time nearby the cluster position is depicted in Fig. 5. The DPL heat transfer model has been implemented in comparison to the Pennes model to compute the thermal behavior of tissues during the laser heating. For DPL model, in both the schemes of IV and IT, a lag in stiff temperature variation has been revealed at the instant of laser on and off as revealed in Fig. 5 (Row 2), due to the limited speed of thermal wavefront. On the other hand, this lag of the stiff temperature variation has not been witnessed in the case of Fourier-based model. Considering the IV scheme, the temperature magnitude at the upper surface of tissue touches the ablation limit ($\geq 51°C$) in lesser time with respect to the IT scheme as shown in Fig. 5. The homogenous spreading of nanoparticles during IV scheme

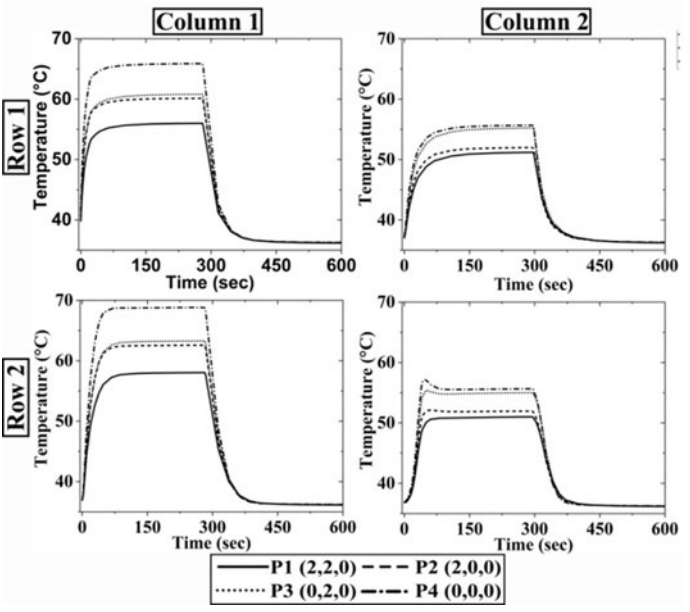

Fig. 5 Temporal plots of temperature at different locations of tissue top surface, viz. P1, P2, P3 and P4, considering the schemes of IV [Column 1] and IT [Column 2] applying the Pennes [Row 1] and DPL [Row 2] model

affects a higher photonic energy immersion at the tissue top surface, in contrast to the IT scheme. For the DPL model, a fluctuation in thermal plot with respect to time has been revealed in the scheme of IT (shown in Fig. 5 [Column 2, Row 2]) prior to achieving the equilibrium condition. The main reason behind this incident is because of the nonhomogeneous tissue structure embedded in clusters of AuNp and also due to the consideration of very small magnitude [17] of 0.043 s as well as a very high magnitude of 16 s. Moreover, no fluctuation in thermal plot has been revealed in the scheme of IV considering DPL model, as shown in Fig. 5 (Column 1, Row 2).

4 Conclusion

A computational study of the thermal behavior of triple-layered tissue structure during laser-based tumor necrosis process has been done signifying the heat sink effect of large blood vessel. To attain a target-specific ablation with minimum healthy tissue damage, considering the countercurrent blood flow, cases like intravenous (IV) and intratumoral (IT) doping of nanoparticles have been applied in the present study. For the fixed protocol parameters, the IT scheme witnessed a more uniform necrotic temperature and damage history to the entire tumor regime preserving the surrounding healthy tissue, in contrast to the IV scheme. A lag in thermal responses has been witnessed in the DPL scheme for both the IV and IT cases, whereas the fluctuating behavior of thermal history has been depicted only in the scheme of IT. However, the non-Fourier thermal nature of tissue structure slowly decreases far away from the laser spot. During photothermal lesion ablation process, the effect of stratum corneum layer of skin is reflected by the differences in temperature plot at different layers of dermis, epidermis and subcutaneous. All, the non-Fourier bioheat model-based thermal prediction of tissue medium allows a more accurate result than the classical Pennes model.

References

1. Maltzahn, G. V., Park, J., Agarwal, A., Bandaru, N. K., Das, S. K., Sailor, M. J., & Bhatia, S. N. (2009). Computationally guided photothermal tumor therapy using long-circulating gold nanorod antennas. *Cancer Research, 69*(9), 3892–3900.
2. Sayed, M. A., Shabaka, A. A., El-Shabrawy, O. A., N.A. Yassin, N. A., Mahmoud, S. S., El-Shenawy, S. M., Al-Ashqar, E., Eisa, W. H., Farag, N. M., El-Shaer, M. A., et al. (2013). Tissue distribution and efficacy of gold nanorods coupled with laser induced photoplasmonic therapy in ehrlich carcinoma solid tumor model. *PLOS One, 8*(10), e76207 1–9.
3. Ren, Y., Qi, H., Chen, Q., & Ruan, L. (2017). Thermal dosage investigation for optimal temperature distribution in gold nanoparticle enhanced photothermal therapy. *International Journal of Heat and Mass Transfer, 106*, 212–221.
4. Dua, R., & Chakraborty, S. (2005). A novel modeling and simulation technique of photo–thermal interactions between lasers and living biological tissues undergoing multiple changes in phase. *Computers in Biology and Medicine, 35*, 447–462.

5. Jaunich, M., Raje, S., Kim, K., Mitra, K., & Guo, Z. (2008). Bio-heat transfer analysis during short pulse laser irradiation of tissues. *International Journal of Heat and Mass Transfer, 51*(23–24), 5511–5521.
6. Paul, A., Narasimahan, A., Kahlen, A., & Das, S. K. (2014). Temperature evolution in the tissues embedded with large blood vessels during photo-thermal heating. *Journal of Thermal Biology, 41*, 77–87.
7. Kumar, S., & Srivastava, A. (2015). Thermal analysis of laser-irradiated tissue phantoms using dual phase lag model coupled with transient radiative transfer equation. *International Journal of Heat and Mass Transfer, 90*, 466–479.
8. Kumar, S., & Srivastava, A. (2017). Finite integral transform-based analytical solutions of dual phase lag bio-heat transfer equation. *Applied Mathematical Modelling, 52*, 378–403.
9. Wongchadakul, P., Rattanadecho, P., & Wessapan, T. (2018). Implementation of a thermo-mechanical model to simulate laser heating in shrinkage tissue (effects of wavelength, laser irradiation intensity, and irradiation beam area). *International Journal of Thermal Sciences, 134*, 321–326.
10. Paul, A., & Paul, A. (2018). Computational study of photo-thermal ablation of large blood vessel embedded tumor using localized injection of gold nanoshells. *Journal of Thermal Biology, 78*, 329–342.
11. Paul, A., & Paul, A. (2019). Thermomechanical analysis of a triple layered skin structure in presence of nanoparticle embedding multi-level blood vessels. *International Journal of Heat and Mass Transfer, 148*, 119076. https://doi.org/10.1016/j.ijheatmasstransfer
12. Paul, A., & Paul, A. (2020). In-vitro thermal assessment of vascularized tissue phantom in presence of gold nanorods during photo-thermal therapy. *Journal of Heat Transfer ASME*. https://doi.org/10.1115/1.4047371
13. Cetingul, M. P., & Herman, C. (2011). Quantification of the thermal signature of melanoma lesion. *International Journal of Thermal Science, 50*, 421–431.
14. Wang, X., Gao, X., & Liu, J. (2010). Monte-Carlo simulation on gold nanoshells enhanced laser interstitial thermal therapy on target tumor. *Journal of Computational and Theoratical Nanoscience, 7*, 1025–1031.
15. Saccomandi, P., Schena, E., Caponero, M. A., Di Matteo, F. M., Martino, M., Pandolfi, M., et al. (2012). Theoretical analysis and experimental evaluation of laser-induced interstitial thermotherapy in ex vivo porcine pancreas. *IEEE Transactions on Biomedical Engineering, 59*(9), 2958–2964.
16. Welch, A. J. (1984). The thermal response of laser irradiation tissue. *IEEE Journal of Quantum Electronics, 20*(12), 1471–1481.
17. Patidar, S., Kumar, S., Srivastava, A., & Sing, S. (2016). Dual phase lag model-based thermal analysis of tissue phantoms using lattice Boltzmann method. *International Journal of Thermal Science, 103*, 41–56.